

**Contract No:**

This document was prepared in conjunction with work accomplished under Contract No. 89303321CEM000080 with the U.S. Department of Energy (DOE) Office of Environmental Management (EM).

**Disclaimer:**

This work was prepared under an agreement with and funded by the U.S. Government. Neither the U.S. Government or its employees, nor any of its contractors, subcontractors or their employees, makes any express or implied:

- 1 ) warranty or assumes any legal liability for the accuracy, completeness, or for the use or results of such use of any information, product, or process disclosed; or
- 2 ) representation that such use or results of such use would not infringe privately owned rights; or
- 3) endorsement or recommendation of any specifically identified commercial product, process, or service.

Any views and opinions of authors expressed in this work do not necessarily state or reflect those of the United States Government, or its contractors, or subcontractors.

We put science to work.™



**Savannah River  
National Laboratory®**

OPERATED BY SAVANNAH RIVER NUCLEAR SOLUTIONS

A U.S. DEPARTMENT OF ENERGY NATIONAL LABORATORY • SAVANNAH RIVER SITE • AIKEN, SC

# Final Report for PDRD SR18010

*Photo-cleaned Backgroundless Ion Chambers*

**George Larsen**

**Simona Murph**

**Khai Nguyen**

September 2020

SRNL-STI-, Revision 0

SRNL.DOE.GOV

## **DISCLAIMER**

This work was prepared under an agreement with and funded by the U.S. Government. Neither the U.S. Government or its employees, nor any of its contractors, subcontractors or their employees, makes any express or implied:

1. warranty or assumes any legal liability for the accuracy, completeness, or for the use or results of such use of any information, product, or process disclosed; or
2. representation that such use or results of such use would not infringe privately owned rights; or
3. endorsement or recommendation of any specifically identified commercial product, process, or service.

Any views and opinions of authors expressed in this work do not necessarily state or reflect those of the United States Government, or its contractors, or subcontractors.

**Printed in the United States of America**

**Prepared for  
U.S. Department of Energy**

**Keywords:** *Tritium, Radiation Detectors,  
Decontamination*

**Retention:** *Permanent*

## **Final Report for PDRD SR18010 Photo-cleaned Backgroundless Ion Chambers**

G. K. Larsen  
S. E. H. Murph  
K. V. Nguyen

September 2020

---

Prepared for the U.S. Department of Energy under  
contract number DE-AC09-08SR22470.



## REVIEWS AND APPROVALS

### AUTHORS:

---

G. K. Larsen, Hydrogen Isotope Process Science Date

---

S. E. H. Murph, Energy and Biotechnology Date

---

K. V. Nguyen, Imaging, Robotics & Rad Systems Date

### TECHNICAL REVIEW:

---

K. J. Lawrence, Nuclear Effluent Analysis Date

### APPROVAL:

---

Jose Cortes-Concepcion, Manager Date  
Hydrogen Isotope Process Science

## EXECUTIVE SUMMARY

Ion chambers are often employed to measure the concentration of tritium within flowing gases. In real world environments the active surfaces of ion chambers become covered with tritiated surface contaminants. This tritiated surface contamination will create a large background response that can mask the signature of interest, which is the tritium concentration in the gas phase. Previous efforts to reduce the effects of surface contamination in ion chambers utilize inert coatings (e.g., gold) and low surface area electrodes (e.g., wire mesh), but this route only reduces the effect and does not necessarily alter the ratio of surface contamination to current collection area. Additionally, gold coating may add a substantial cost to the instrument. In the Tritium Facility, ion chambers are periodically cleaned using an alcohol-based process. This process is time consuming and often leads to ion chamber wear and breakage. In addition, periodic cleaning does not address tritium level ambiguities in gloveboxes. An ideal solution to this issue would be to either develop an ion chamber that does not accrue surface contamination, or one that is self-cleaning while it is in operation.

In this report we investigate LED light illumination (UV to near-infrared) to desorb contamination from ion chambers while they are in operation, preventing the appearance of the negative effects of surface contamination. The concept benefits from the rapid improvement in LED technology over the past several years that affords robust, long-lasting, and powerful light sources that can stimulate desorption and are widely available at low cost. The project developed the concept of photo-cleaned backgroundless ion chambers from laboratory investigations of material samples to demonstrating the proof-of-concept in a tritium environment to the construction and tritium testing of a working prototype. Each testing stage revealed significant promise for the concept. Prototype testing in tritium environments demonstrated the main project goal that UV LED integration can be used to promote in situ decontamination of a stainless steel ion chamber while in operation. In addition to the many benefits of a backgroundless ion chamber, this result is also notable because it represents a large potential cost saving by negating the need for gold coatings, and it also suggests that LEDs can be employed to facilitate the detritiation of other stainless-steel surfaces. Future work should focus on fully developing the prototype for operational service and exploring other applications that could benefit from hands free, in situ decontamination using LEDs.

## TABLE OF CONTENTS

LIST OF TABLES .....	vii
LIST OF FIGURES .....	vii
LIST OF ABBREVIATIONS.....	viii
1.0 Introduction.....	1
2.0 Proof-of-Concept Tritium Tests.....	2
2.1 Overview .....	2
2.2 Results and Discussion.....	3
2.3 Conclusions .....	5
3.0 Prototype LED Integrated Ion Chamber .....	5
3.1 Overview .....	5
3.2 Construction .....	5
3.3 Tritium Testing.....	8
3.4 Conclusion.....	8
4.0 Summary and Future Work.....	9
5.0 References.....	10
Appendix A . Representative QCM and FTIR Experiments.....	A-1
Appendix B . Necessary Illumination Intensity for Glovebox Conditions .....	B-4
Appendix C . Nanoparticle Testing.....	C-5
Appendix D . References for the Appendices.....	D-7

## LIST OF TABLES

Table 2-1. Experimental conditions and decay constants obtained through fitting ..... 4

## LIST OF FIGURES

Figure 1-1. Schematic illustrating the concept of a photo-cleaned ion chamber ..... 2

Figure 2-1. Photographs of the ion chamber test stand: (a) shows the tee-shaped vessel and the handheld UV system mounts; (b) shows the gold coated ion chamber inside test vessel; and (c) shows the ion chamber under UV LED illumination ..... 3

Figure 2-2. IC current versus time during the purging experiments (a) under UV LED illumination and (b) in the dark. .... 3

Figure 2-3. IC current versus time during the purging experiments showing the distinctive “kink” for tests conducted both before and after the UV experiments. .... 4

Figure 2-4. Comparisons between the different decay constants for the different tests: (a) plots the second decay region normalized by the first decay region,  $\tau_2/\tau_1$ , for each run; (b) plots the first decay region normalized by the reference IC,  $\tau_1/\tau_{ref}$ , for each run; (c) plots the second decay region normalized by the reference IC,  $\tau_2/\tau_{ref}$ , for each run..... 5

Figure 3-1. Computer-aided design (CAD) drawing bird cage ion chamber on mounting plate..... 6

Figure 3-2. CAD cross-section of ion chamber inside of testing vessel. Three star-shaped LED mounts can be seen: one at the top and two at the bottom. .... 6

Figure 3-3. Photographs of one of the prototype LED integrated ion chambers during assembly and at completion ..... 7

Figure 3-4. Plot of ion chamber current versus time during purging experiments for the (a) dark and (b) UV LED experiments. (c) Direct comparison between selected dark and UV experiments ..... 8

## LIST OF ABBREVIATIONS

BIXS	Beta induced X-ray spectrometry
CAD	Computer-aided design
FTIR	Fourier-transform infrared (spectroscopy)
IC	Ion chamber
LED	Light emitting diode
SEM	Scanning electron microscopy
SRNL	Savannah River National Laboratory
QCM	Quartz crystal microbalance
UV	Ultraviolet

## 1.0 Introduction

Radiation detectors may suffer from “memory effects.” Memory effects means that the radioactive material may interact in some way with, and be retained by, the detector. The detector may respond to radioactive material that is retained, thus providing a response even though the air currently being monitored contains no radioactive materials. The detector “remembers” the radiation in the previous air [1]. While any radiation detector may experience memory effects due to surface contamination, the following detectors are well-known in the literature to experience such effects:

1. Gaseous ionization detectors (ion chambers, proportional counters, Geiger counters) [2, 3],
2. Scintillation detectors, both organic and inorganic [4, 5],
3. Beta induced X-ray spectrometry (BIXS) [6].

In addition, non-radioactive surface contamination from water and absorbed species can negatively affect radiation detectors. For example, stray current can leak across the surfaces of insulators that are covered with non-radioactive contamination, leading to higher background signals in gaseous ionization detectors [7]. Thus, the performance of radiation detectors could be improved and memory effects could be eliminated by removing both non-radioactive and radioactive contamination from detector surfaces while in operation.

Ion chambers are often employed to measure the concentration of tritium within flowing gases. The basic concept is straightforward: tritium decay ionizes background gas molecules, and these ionized molecules produce a current within an applied electric field. This ionic current is measured providing an electrical readout of the tritium concentration. However, in real world environments the active surfaces of ion chambers become covered with a variety of tritiated and easily tritiated surface contaminants. This tritiated surface contamination will contribute to the measured current of the ion chamber, creating a large background response that can mask the signature of interest, which is the tritium concentration in the gas phase. This is the memory effect described above, and it is especially problematic for the detection of tritium due to isotopic exchange in surface contamination.

Previous efforts to reduce the effects of surface contamination in ion chambers utilize low surface area electrodes (*e.g.*, wire mesh),[8] but this route only reduces the effect and does not necessarily alter the ratio of surface contamination to current collection area. Currently, ion chambers in the Tritium facility are periodically cleaned using an alcohol-based process. This process is time consuming and often leads to ion chamber wear and breakage. In addition, periodic cleaning does not address tritium level ambiguities in gloveboxes. An ideal solution to this issue would be to either develop an ion chamber that does not accrue surface contamination, or one that is self-cleaning while it is in operation. Furthermore, the mechanism should work equally well for hydrophobic and hydrophilic molecules due to the potential for contamination from both.

In this report we investigate LED light illumination (UV to near-infrared) to desorb contamination from ion chambers while they are in operation, preventing the appearance of the negative effects of surface contamination (**Figure 1-1**). The concept is based on recently published studies showing that UV light illumination can be used to remove surface contamination and create atomically clean metal surfaces for devices.[9, 10] The concept also benefits from the rapid improvement in LED technology over the past several years that affords robust, long-lasting, and powerful light sources that can stimulate desorption and are widely available at low cost. We also investigate the potential of metal nanoparticles for this process since they interact more strongly with light than their bulk counterparts, and therefore, could show a greater efficiency for photo-removal of surface adsorbed species.[11]

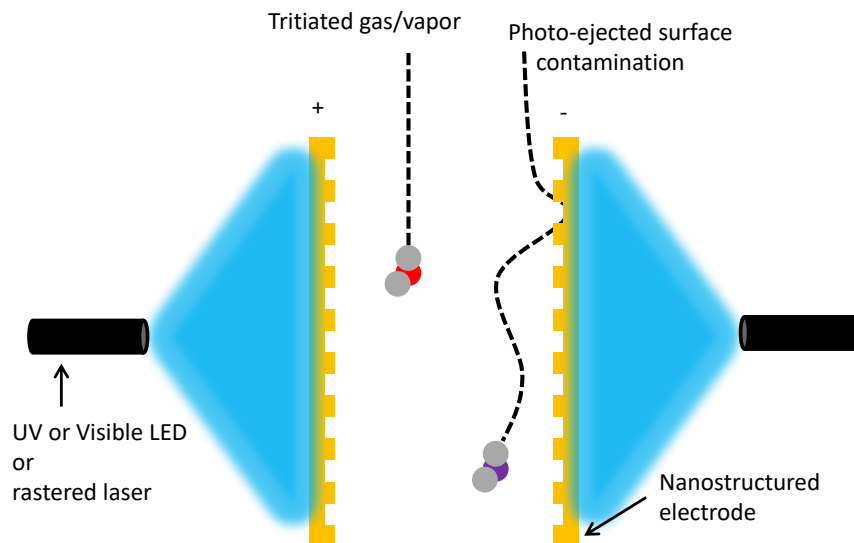


**Figure 1-1. Schematic illustrating the concept of a photo-cleaned ion chamber**

The project focused on the development of a working ion chamber with integrated LEDs and subsequent tritium testing. Therefore, this report will describe the demonstration of the proof-of-concept and the construction and testing of the prototype ion chamber. Throughout this project the research was augmented by laboratory experiments of light-material interactions. Summaries of these lab experiments and representative data are included in the attached appendices.

## 2.0 Proof-of-Concept Tritium Tests

### 2.1 Overview

Initial testing of in situ photo-cleaning employed an existing gold coated “bird cage” style of ion chamber and an existing ion chamber calibration manifold. The calibration manifold was adapted to include a quartz window for illuminating the ion chamber externally from the side (**Figure 2-1**). Additionally, a test stand was assembled to support the new larger vessel that contains the ion chamber and to hold a ThorLabs spot curing UV LED system. The LED central wavelength is  $\lambda = 365 \text{ nm}$ , which outputs a maximum power of  $135 \text{ mW/cm}^2$  at the focus. However, the power delivered in this setup is significantly less since the ion chamber is placed at large distance from the focus in order to obtain an even spread of light illumination across its surface.

The basic test procedure consists of exposing the manifold to trace levels of tritium within a nitrogen background at 1 atm for a set amount of time. Afterward, the tritium source is closed, and the manifold is purged. The purge gas consists of room air at 1 atm that is pulled in by a vacuum pump. The manifold contains both a reference ion chamber and a birdcage ion chamber. The birdcage ion chamber is either left in the dark or illuminated by the UV LED as shown in Figure 2-1 for dark and UV experiments, respectively. The reference ion chamber is based on a spherical design and remains in the dark for all experiments. The radiation induced currents for both ion chambers are monitored during the purge procedure by a picoammeter. The relatively low level of light illumination used in the UV experiments did not induce a noticeable response in the picoammeter. Initial shakedown tests highlighted the need for minor changes in the manifold set up (Tests 1 – 4). Test 5 and beyond (11 tests were conducted) produced consistent results, which will be discussed below.

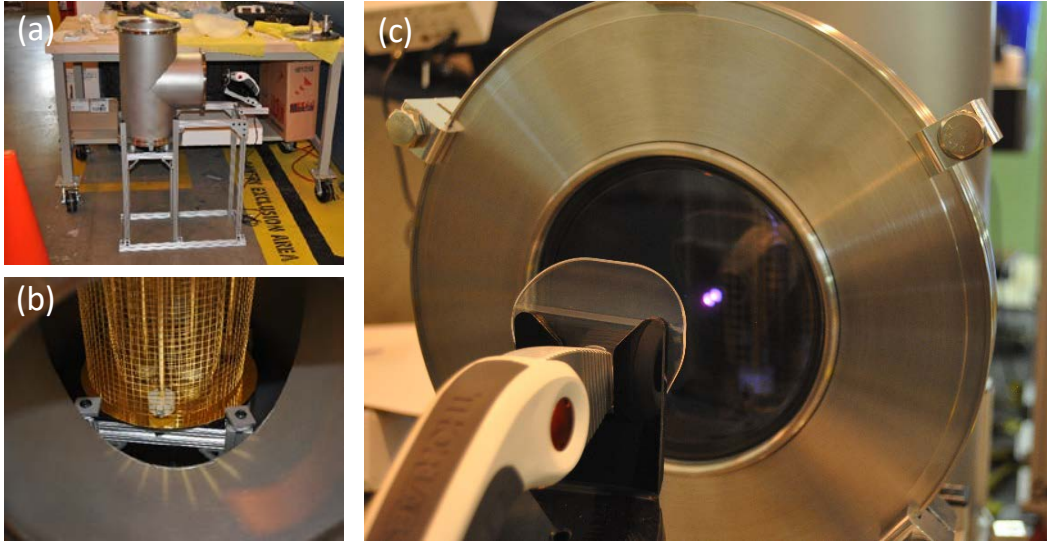


**Figure 2-1. Photographs of the ion chamber test stand: (a) shows the tee-shaped vessel and the handheld UV system mounts; (b) shows the gold coated ion chamber inside test vessel; and (c) shows the ion chamber under UV LED illumination**

## 2.2 Results and Discussion

The results of the experiments are presented in **Figure 2-2**, which plots the ion chamber (IC) current versus time during the purge procedure for both the UV and dark experiments. The overall change in the IC current versus time depends on a number of variables including temperature, humidity, previous history, and minor adjustments at the start of each test. Thus, there are experimental variations which contribute to how quickly the IC current approaches background in addition to that of UV LED illumination. However, the UV illuminated purges exhibit a noticeably faster recovery to baseline, except for Test 6, which may have been affected by a buildup of contamination from the previous five dark experiments.

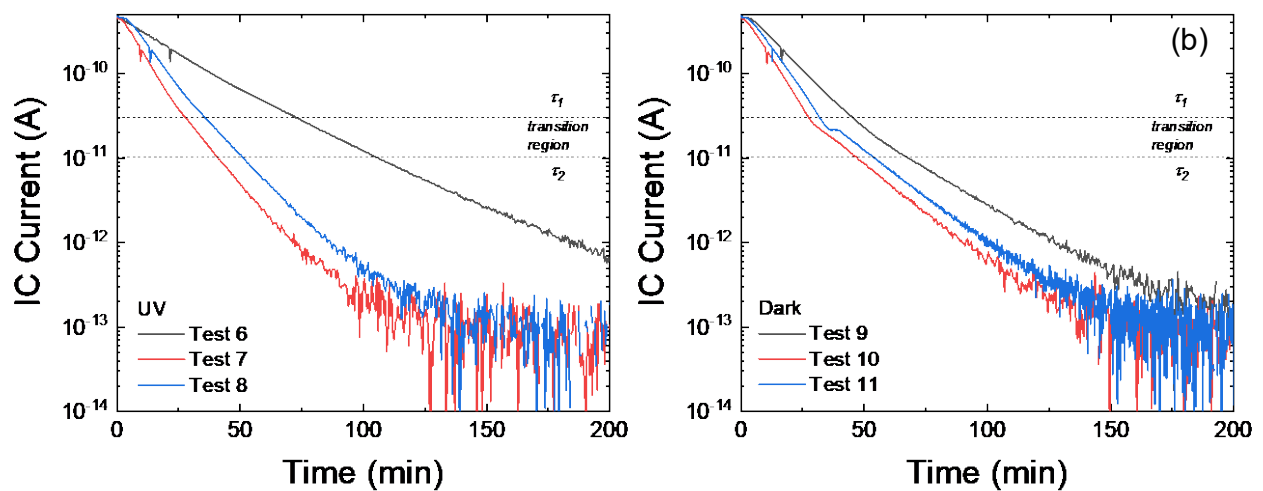


**Figure 2-2. IC current versus time during the purging experiments (a) under UV LED illumination and (b) in the dark.**

In all of the plots, the change in the IC current appears to have two different regions: an initial decay region and a second decay region, with a slightly variable transition between them. The tritium in gas phase is expected to predominate the signal in the initial decay region as tritium is purged and physisorbed tritium is desorbed from surfaces throughout the manifold, including the ion chamber. The tritium contamination on the ion chamber surface will have a larger effect in the second decay region. For the dark experiments, the decay in the second region is notably much slower, which is also observed by a characteristic kink in the plots. This feature is clearly observed in all of the dark experiments, but only subtly in the UV experiments. It is also observed in dark tests that preceded the UV experiment (**Figure 2-3**), and thus, is specific to the dark experiments and not the UV.

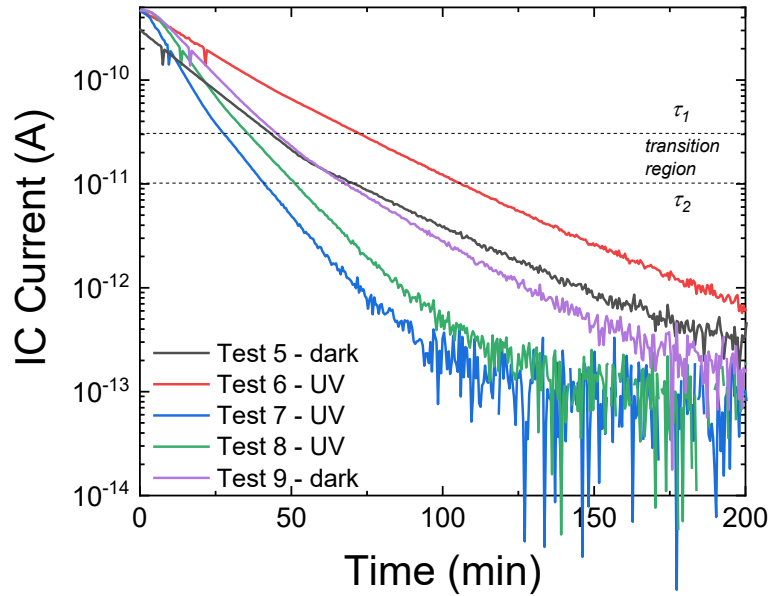


**Figure 2-3. IC current versus time during the purging experiments showing the distinctive “kink” for tests conducted both before and after the UV experiments.**

In order to quantitatively compare the results from the experiments, the different data sets were fit to an exponential decay equation:  $I(t) = A \text{Exp}[-t/\tau_n] + I_0$ , where  $\tau_n$  is the corresponding decay constant,  $A$  is a constant related to the initial current, and  $I_0$  corresponds with the baseline current. The Reference IC current was fit to a single exponential decay with  $\tau_{\text{ref}}$  as the decay constant. The birdcage IC current was fit to two different exponential decays, one covering the first region and the other covering the second, lower current region. The exponential time constants for these two different regions are  $\tau_1$  and  $\tau_2$ , respectively. The fitting results are presented in the **Table 2-1**.

Table 2-1. Experimental conditions and decay constants obtained through fitting

	UV LED	Humidity (%)	$\tau_{\text{ref}}$ (1/min)	$\tau_1$ (1/min)	$\tau_2$ (1/min)	$\tau_2 / \tau_1$	$\tau_1 / \tau_{\text{ref}}$	$\tau_2 / \tau_{\text{ref}}$
Test 6	On, t = 700s	46.1	$1.21 \pm 0.01$	$23.4 \pm 0.2$	$29.9 \pm 0.1$	$1.28 \pm 0.01$	$19.2 \pm 0.3$	$24.6 \pm 0.3$
Test 7	On, t = 0s	52.3	$0.73 \pm 0.05$	$8.8 \pm 0.2$	$11.9 \pm 0.1$	$1.35 \pm 0.03$	$12.0 \pm 0.8$	$16 \pm 1$
Test 8	On, t = 0s	55.5	$1.0 \pm 0.1$	$11.1 \pm 0.2$	$13.9 \pm 0.1$	$1.25 \pm 0.03$	$11 \pm 1$	$14 \pm 1$
Test 9	Off	57.5	$0.89 \pm 0.03$	$14.6 \pm 0.2$	$23.1 \pm 0.1$	$1.58 \pm 0.03$	$16.6 \pm 0.5$	$26.2 \pm 0.8$
Test 10	Off	55.2	$0.72 \pm 0.03$	$10.4 \pm 0.3$	$18.1 \pm 0.1$	$1.73 \pm 0.04$	$14.4 \pm 0.7$	$25 \pm 1$
Test 11	Off	52.2	$0.72 \pm 0.01$	$11.3 \pm 0.1$	$18.9 \pm 0.1$	$1.67 \pm 0.02$	$15.7 \pm 0.3$	$26.2 \pm 0.4$

The experimental variation between each run can be minimized by comparing the different time constants within each test run. **Figure 2-4a** plots  $\tau_2/\tau_1$  and demonstrates that the time constants  $\tau_1$  and  $\tau_2$  are more similar for the UV tests than for the dark tests. This can be seen by visual inspection of Figure 2-3 – there is a noticeable transition for the dark and not UV. **Figure 2-4b** compares  $\tau_1/\tau_{ref}$  and shows that the initial decay region is generally faster for the UV tests and improves with increasing UV exposure. Note that Test 6 had a 700s delay before the UV light was turned on. The dark experiments fluctuate around the same value. **Figure 2-4c** compares  $\tau_2/\tau_{ref}$  and demonstrates that second decay region when normalized by  $\tau_{ref}$  is always faster for the UV tests. Again, the dark experiments fluctuate around the same value, while improvement is observed for increasing UV exposures. The second decay region is expected to be more sensitive to surface contamination of the IC.

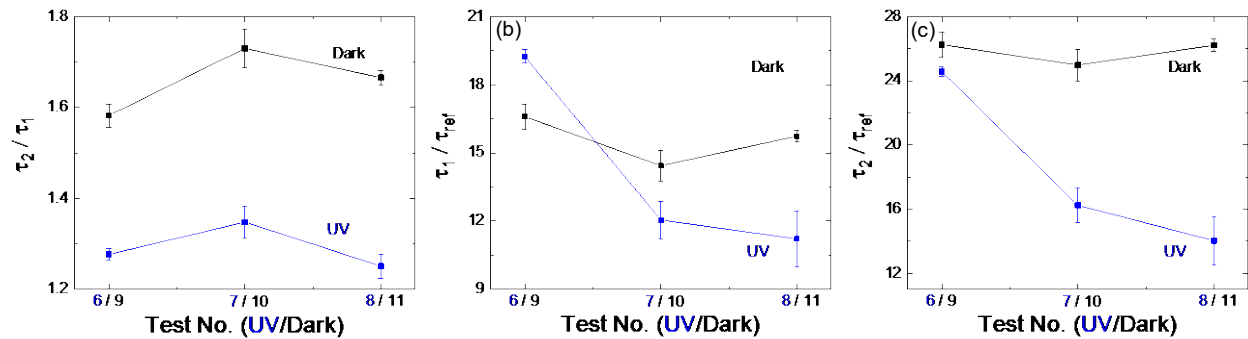


**Figure 2-4. Comparisons between the different decay constants for the different tests: (a) plots the second decay region normalized by the first decay region,  $\tau_2/\tau_1$ , for each run; (b) plots the first decay region normalized by the reference IC,  $\tau_1/\tau_{ref}$ , for each run; (c) plots the second decay region normalized by the reference IC,  $\tau_2/\tau_{ref}$ , for each run**

### 2.3 Conclusions

The results described above are promising and show that a single UV LED mounted on the outside of a test assembly can stimulate faster recovery and a lower baseline for a bird cage ion chamber. The observed effects are attributed to the photo-effects of UV illumination, as the relatively low level of illumination would not generate any appreciable thermal effects, and are supported by laboratory measurements (Appendix A) Thus, the proof-of-concept of a photo-cleaned ion chamber has been established.

## 3.0 Prototype LED Integrated Ion Chamber

### 3.1 Overview

The promising results described in Section 2 motivated the construction and assembly of prototype ion chambers with integrated LEDs that can enable in situ photo-decontamination of the surface. Two ion chambers were constructed, one which could be mounted inside of the test manifold described above and another that can be installed in a Tritium Facility glovebox for validation within its intended application.

### 3.2 Construction

The design of the ion chambers is based on the original bird cage design. However, one notable change is that the ion chambers will use uncoated stainless-steel surfaces instead of gold coated ones. Gold coating adds a significant cost (estimated as much as \$100k) to the ion chamber construction, which is cost-prohibitive for the current project. Furthermore, demonstrating the ability to photo-clean stainless-steel ion

chambers using LEDs would represent a large cost savings by reducing the reliance on gold coatings to achieve low backgrounds and reduce the memory effect of surface contamination.

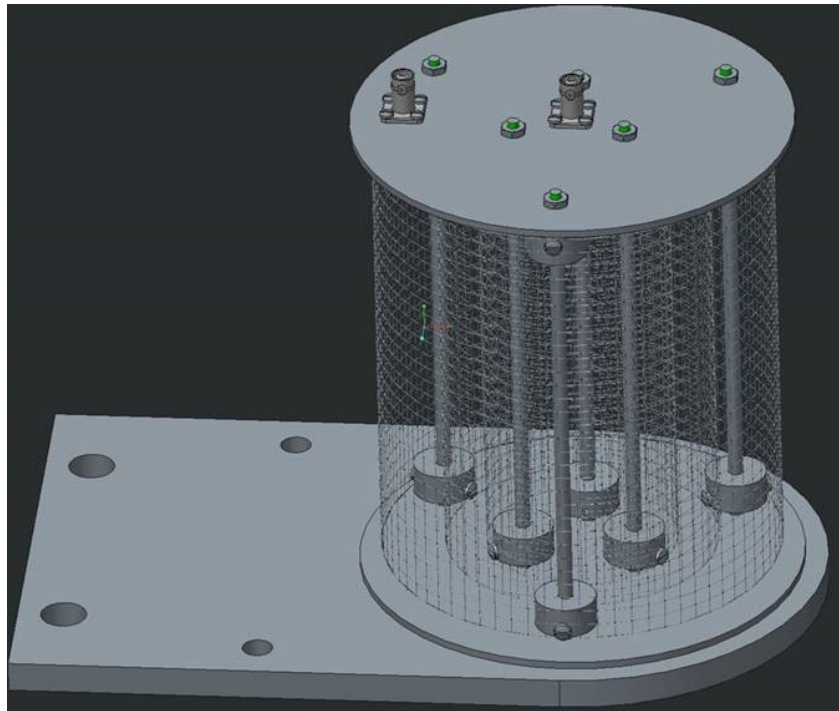


**Figure 3-1. Computer-aided design (CAD) drawing bird cage ion chamber on mounting plate.**

The bird cage design has also been updated for two different mounting brackets (**Figure 3-1**), one for glovebox testing and one for testing in the calibration manifold. Most importantly, the ion chamber design was modified to accept LED light integration. In this case, 6 LEDs with center wavelengths of 365 nm are mounted on the outer plates of the ion chambers. Each plate holds three LEDs placed at 120° intervals, with the opposing plates offset by 60° to ensure uniform coverage on the electrode mesh (**Figure 3-2**).

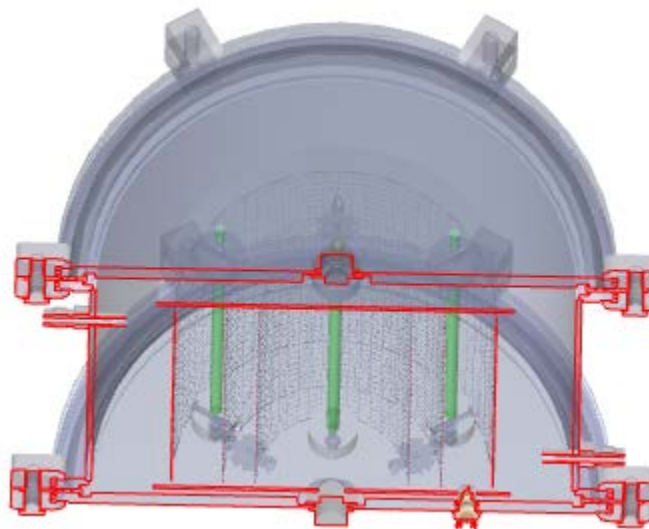


**Figure 3-2. CAD cross-section of ion chamber inside of testing vessel. Three star-shaped LED mounts can be seen: one at the top and two at the bottom.**

Each LED is capable of outputs of 810 mW at a minimum with a viewing angle of 130°. The illumination capacity of the prototypes is intended to far exceed the needed capacity expected for successful operation since one LED mounted at a distance was capable of generating noticeable results, as described above, and also exceeds estimates predicted by lab experiments (Appendix B). The idea is that the additional capabilities of these experimental devices will allow for greater understanding and optimization of the final device.

The prototypes have been assembled and are ready for testing, as shown in **Figure 3-3**. The final tritium testing of the prototypes will be conducted after the completion of this report.



**Figure 3-3. Photographs of one of the prototype LED integrated ion chambers during assembly and at completion**

### 3.3 Tritium Testing

The tritium testing of the prototype followed the same test procedure used for the proof-of-concept, described in Section 2.1 above. The basic procedure involves exposing the ion chamber to a recirculating tritium/nitrogen gas mixture, followed by purging using room air pulled through a vacuum and out the stack to create air flow while maintaining pressure slightly below ambient. Seven purging tests were performed. The first purge (Test 1) was done under UV illumination, followed by three dark tests (Tests 2 - 4) and three UV tests (Test 5 - 7). Background measurements were also taken with UV LEDs both on and off to observe any effects on the steady-state current of the ion chamber, and none were observed.

The data for Tests 1 - 7 are presented in **Figure 3-4**. The results are similar to those of the proof-of-concept testing. The dark experiments have similar or increasing background currents for increasing test cycles. In comparison, each UV exposure reduces the background current, eventually to where the background disappears. Additionally, the initial UV experiments reach background faster than the dark experiments, and the UV experiments also achieve a lower base current than the dark experiments. A notable difference between these experiments and the proof-of-concept experiments (gold coated) is that these demonstrate the effectiveness of UV LED light for the in-situ decontamination of stainless-steel surfaces.

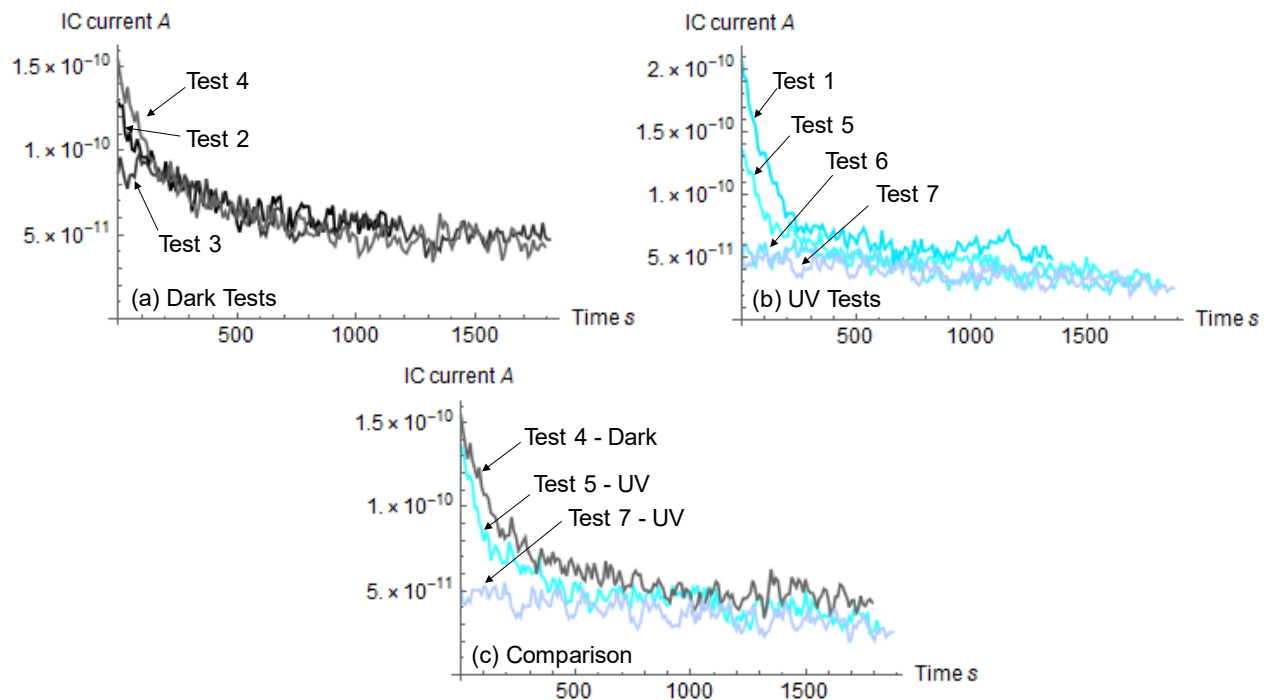


**Figure 3-4. Plot of ion chamber current versus time during purging experiments for the (a) dark and (b) UV LED experiments. (c) Direct comparison between selected dark and UV experiments**

### 3.4 Conclusions

Initial tritium testing of the tritium testing of the first LED integrated ion chamber prototype was conducted. This is the first reported demonstration of this technology concept. The results showed stainless steel surfaces illuminated by UV LEDs are decontaminated faster than non-illuminated stainless-steel surfaces. They also demonstrated that the light illumination reduced the accumulation of ion chamber background signal after exposure to tritium. Thus, the LED integrated system functions as a backgroundless ion chamber.

#### **4.0 Summary and Future Work**

The project developed the concept of photo-cleaned backgroundless ion chambers from laboratory investigations of material samples to demonstrating the proof-of-concept in a tritium environment to the construction and tritium testing of a working prototype. Each testing stage revealed significant promise for the concept. Prototype testing in tritium environments demonstrated the main project goal that UV LED integration can be used to promote in situ decontamination of a stainless-steel ion chamber while in operation. In addition to the many benefits of a backgroundless ion chamber, this result is also notable because it represents a large potential cost saving by negating the need for gold coatings, and it also suggests that LEDs can be employed to facilitate the detritiation of other stainless-steel surfaces. Future work should focus on fully developing the prototype for operational service and exploring other applications that could benefit from hands free, in situ, and rapid decontamination using LEDs.

## 5.0 References

1. Traub, R. and G. Jensen, *Tritium radioluminescent devices*, *Health and Safety Manual*. 1995, Pacific Northwest Lab., Richland, WA (United States).
2. Nishikawa, M., et al., *Ionization chamber system to eliminate the memory effect of tritium*. Nuclear Instruments and Methods in Physics Research Section A: Accelerators, Spectrometers, Detectors and Associated Equipment, 1989. **278**(2): p. 525-531.
3. Shank, K. and C. Easterly, *Tritium instrumentation for a fusion reactor power plant*. 1976, Oak Ridge National Lab.
4. Seifert, C.E., et al., *Mitigation of memory effects in beta scintillation cells for radioactive gas detection*. Proceedings of the 27th Seismic Research Review: Ground-Based Nuclear Explosion Monitoring Technologies, 2005: p. 804-814.
5. Sheen, S., *NRC Job Code V6060: Extended in-situ and real time monitoring. Task 4: Detection and monitoring of leaks at nuclear power plants external to structures*. 2012, Argonne National Lab.(ANL), Argonne, IL (United States).
6. Röllig, M., et al., *Activity monitoring of a gaseous tritium source by beta induced X-ray spectrometry*. Fusion Engineering and Design, 2013. **88**(6): p. 1263-1266.
7. Knoll, G.F., *Radiation detection and measurement*. 2010: John Wiley & Sons.
8. Worth, L., et al., *Development of a novel contamination resistant ion chamber for process tritium measurement and use in the JET first trace tritium experiment*. Fusion science and technology, 2005. **48**(1): p. 370-373.
9. Vig, J.R., *UV/ozone cleaning of surfaces*. Journal of Vacuum Science & Technology A, 1985. **3**(3): p. 1027-1034.
10. Shu, W.M., et al., *Tritium decontamination of TFTR carbon tiles employing ultra violet light*. Journal of Nuclear Materials, 2001. **290-293**: p. 482-485.
11. Brongersma, M.L., N.J. Halas, and P. Nordlander, *Plasmon-induced hot carrier science and technology*. Nature nanotechnology, 2015. **10**(1): p. 25-34.
12. Zion, B.D. and S.J. Sibener, *UV Photodesorption of Novel Molecular Beam Induced NO Layers on NiO(111)/Ni(111)*. The Journal of Physical Chemistry C, 2008. **112**(15): p. 5961-5965.
13. Owega, S., E.P.C. Lai, and A.D.O. Bawagan, *Surface Plasmon Resonance-Laser Desorption/Ionization-Time-of-Flight Mass Spectrometry*. Analytical Chemistry, 1998. **70**(11): p. 2360-2365.
14. Law, K. and J.R. Larkin, *Recent advances in SALDI-MS techniques and their chemical and bioanalytical applications*. Analytical and bioanalytical chemistry, 2011. **399**(8): p. 2597-2622.

## Appendix A. Representative QCM and FTIR Experiments

A quartz crystal microbalance (QCM) system was employed to measure trace amounts of surface adsorbed species on gold surfaces. QCMs are often used to measure materials at angstrom level ( $10^{-10}$  m) thicknesses. A gold-coated QCM crystal was placed in a vessel and exposed to water vapor saturated ( $22\text{ }^{\circ}\text{C}$ ) flowing  $\text{N}_2$  gas (200 mL/min), and the QCM signal indicated that water was being deposited on the surface of the gold. Next, the gold surface was exposed to LED light illumination while in the flowing  $\text{N}_2$  gas and water vapor. Upon LED light illumination for all wavelengths tested, the mass on the gold surface decreased dramatically (**Figure A-1**), indicating that the light was removing the trace amounts of water that had been adsorbed and absorbed by the gold-coated QCM crystal. Surface water is an important contamination source for radiation detectors, as described above. Additionally, water contamination is especially problematic for tritium (radioactive hydrogen) detection, as isotopic exchange will result in non-radioactive surface water becoming radioactive and producing a background signal (memory effect).

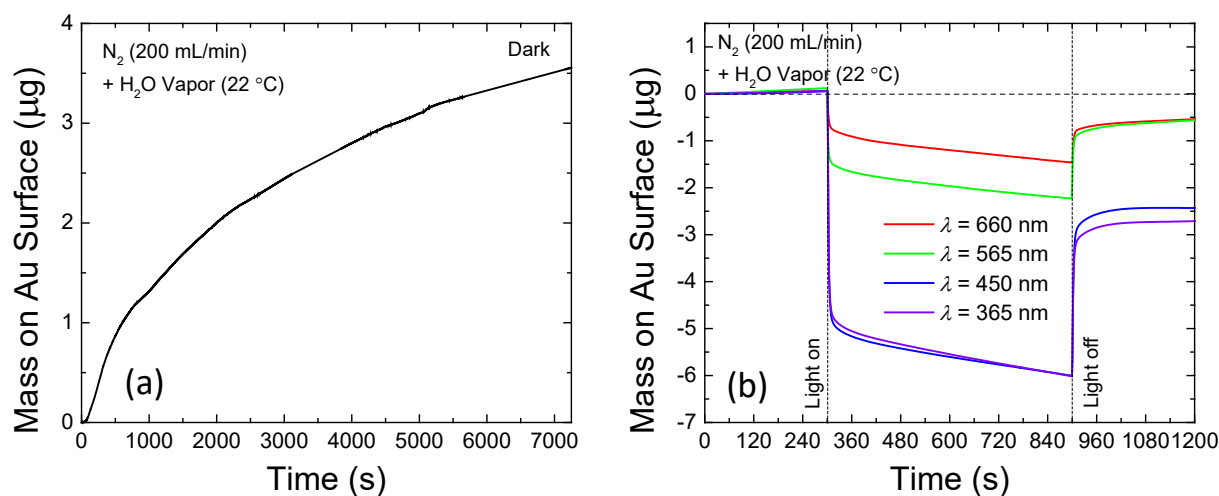


**Figure A-1. (a) QCM trace versus time showing increase in mass on gold surface after water is introduced. (b) QCM traces versus time showing decrease in mass on a water saturated gold surface after LEDs with different wavelengths are turned on/off**

Carbon contamination is also ubiquitous and can lead to leakage currents and background signals from isotopic exchange. Thus, a similar experiment was done to test for carbon-based contamination removal. Mineral oil (a representative, non-volatile hydrocarbon) was pipetted onto the gold-coated QCM crystal, and then placed in the measurement chamber under flowing  $\text{N}_2$  gas (200 mL/min). Again, the contaminated gold surface was exposed to LED light illumination while in the flowing  $\text{N}_2$  gas. For all wavelengths of LED light illumination, the mass on the gold surface decreased (**Figure A-2**), indicating that the light was removing the hydrocarbon contamination that was deposited onto the gold-coated QCM crystal.

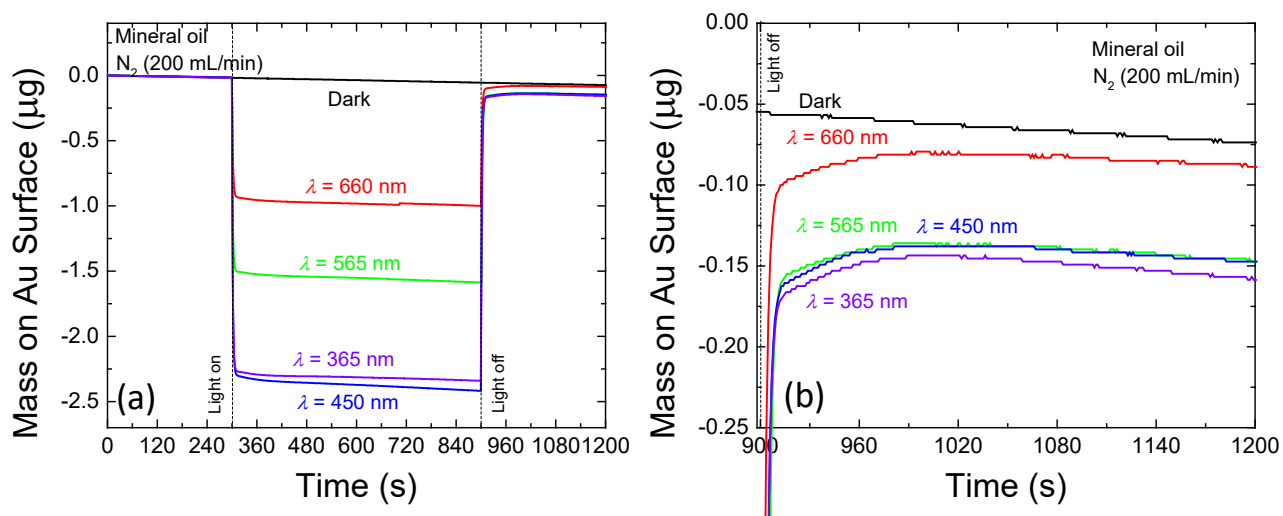


**Figure A-2. (a) QCM traces versus time showing decrease in mass on a hydrocarbon (mineral oil) contaminated gold surface after LEDs with different wavelengths are turned on/off. (b) Closer view of the mass on the gold surface after the LEDs are turned off at 900 s.**

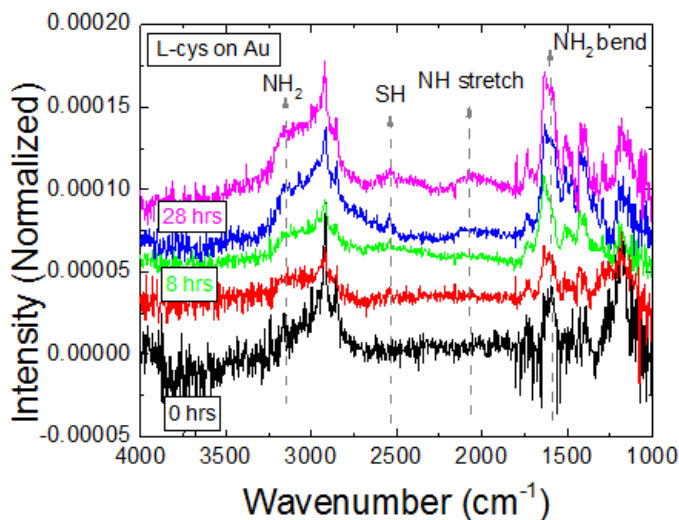


**Figure A-3 . FTIR of *L*-cysteine on gold after different UV LED ( $\lambda = 365$  nm) irradiation times. Increasing peaks are shown. The spectra are offset to improve clarity.**

Fourier-transform infrared (FTIR) spectroscopy can provide insight into the chemical changes occurring in the surface contamination under LED illumination. **Figure A-3** shows the changes in *L*-cysteine that has been adsorbed onto a gold surface and exposed to a UV LED light source. *L*-cysteine serves as a representative chemically adsorbed carbonaceous contamination source. It chemically adsorbs to gold surfaces through thiol (gold-sulfur) and amine (gold-nitrogen) bonds. Therefore, SH, NH, and NH<sub>2</sub> vibrational modes are not seen in the FTIR spectra when *L*-cysteine is chemically bonded to the gold surface. As seen in Figure A-3, initially these vibrational modes are not seen, indicating that the *L*-cysteine is chemically adsorbed on the gold surface. As the illumination time increases, these modes reappear,

revealing that the UV light is breaking the surface chemical bonds of *L*-cysteine. **Figures A-4 and A-5** show the changes in the FTIR spectra in carbon contamination on gold (mineral oil) and stainless steel (native) surfaces under illumination, respectively. These data confirm the QCM data in showing that the LED light illumination removes hydrocarbon contamination from different surfaces.

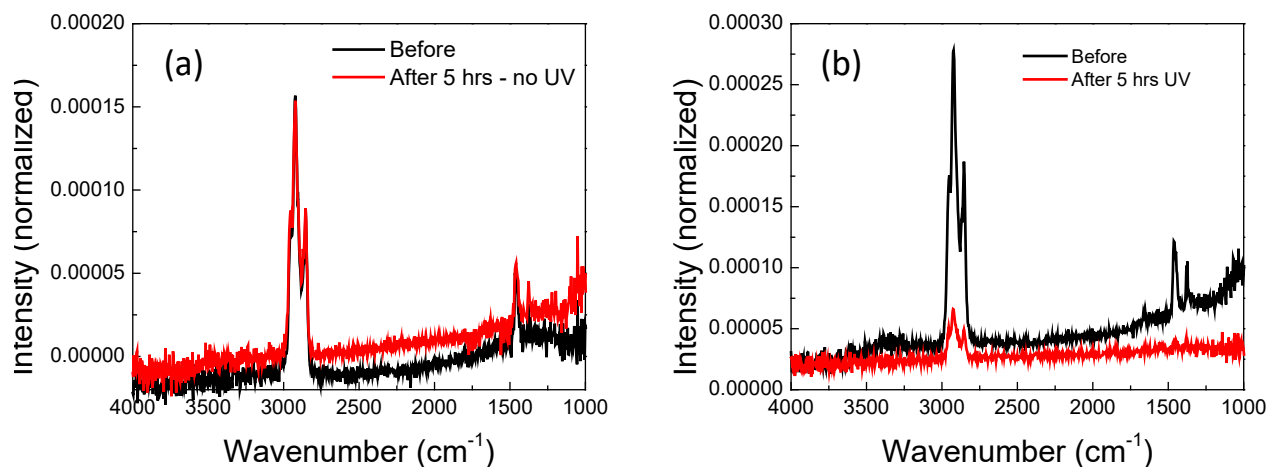


**Figure A-4. (a) FTIR spectra from dark experiment, showing that after 5 hours with no light exposure, the hydrocarbon peaks from mineral oil remain strong. (b) FTIR spectra from LED experiment, showing that after 5 hours of UV LED ( $\lambda = 365$  nm) exposure the hydrocarbon peaks decrease and disappear.**

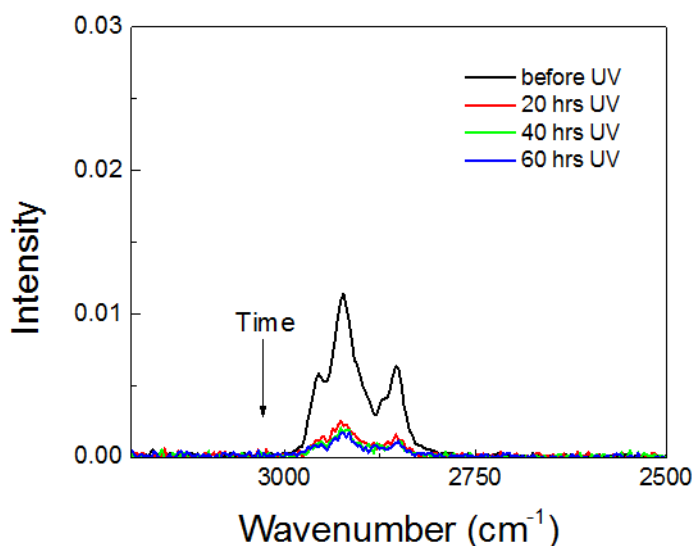


**Figure A-5. Stainless steel coupons contained “native” carbon contamination from processing, as indicated by CH<sub>3</sub> peaks observed in the FTIR spectra. Upon illumination with UV LED ( $\lambda = 365$  nm), these peaks decrease, indicating removal of contamination.**

### Appendix B. Necessary Illumination Intensity for Glovebox Conditions

A quartz crystal microbalance (QCM) system was employed to investigate the necessary illumination conditions to remove surface water from a gold ion chamber surface using a 450 nm LED. A background concentration of 300 ppm H<sub>2</sub>O would impart a molecular flux of 3.2 micrograms/cm<sup>2</sup> s to any exposed surface. However, not all H<sub>2</sub>O molecules striking the surface will remain there, as determined by the sticking probability of the surface. The sticking probability for gold surfaces is very low, and in our experiments, we measure it to be  $S = 5.48 \times 10^{-6}$  by measuring the mass gain rate in H<sub>2</sub>O flow. Thus, at 300 ppm, the necessary H<sub>2</sub>O removal rate needs to be  $1.76 \times 10^{-5}$  micrograms/cm<sup>2</sup> s. For the smallest experimental value of illumination intensity, 13 mW, we measure a removal rate of  $2.28 \times 10^{-4}$  micrograms/cm<sup>2</sup> s (**Figure B-1**). Thus, we need to deliver  $\sim 1$  mW/cm<sup>2</sup> to remove all surface water from a gold surface at 300 ppm using a 450 nm LED.

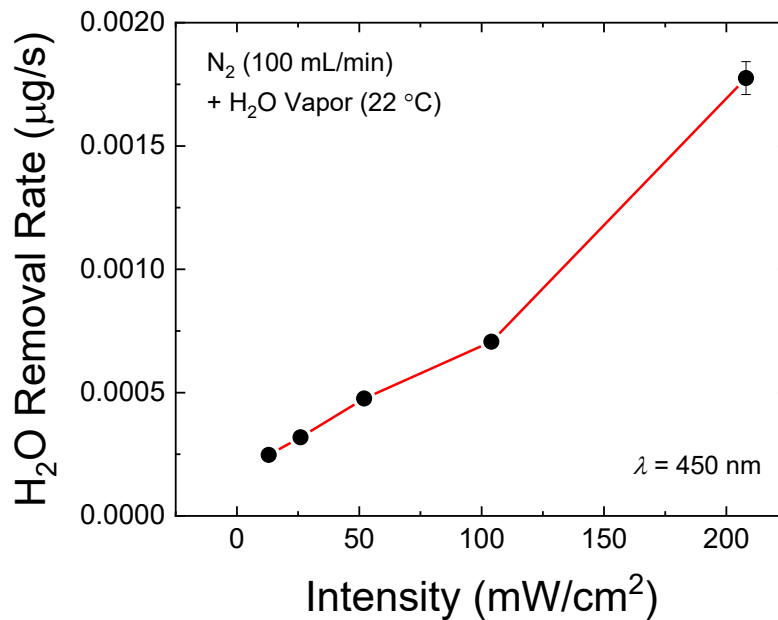
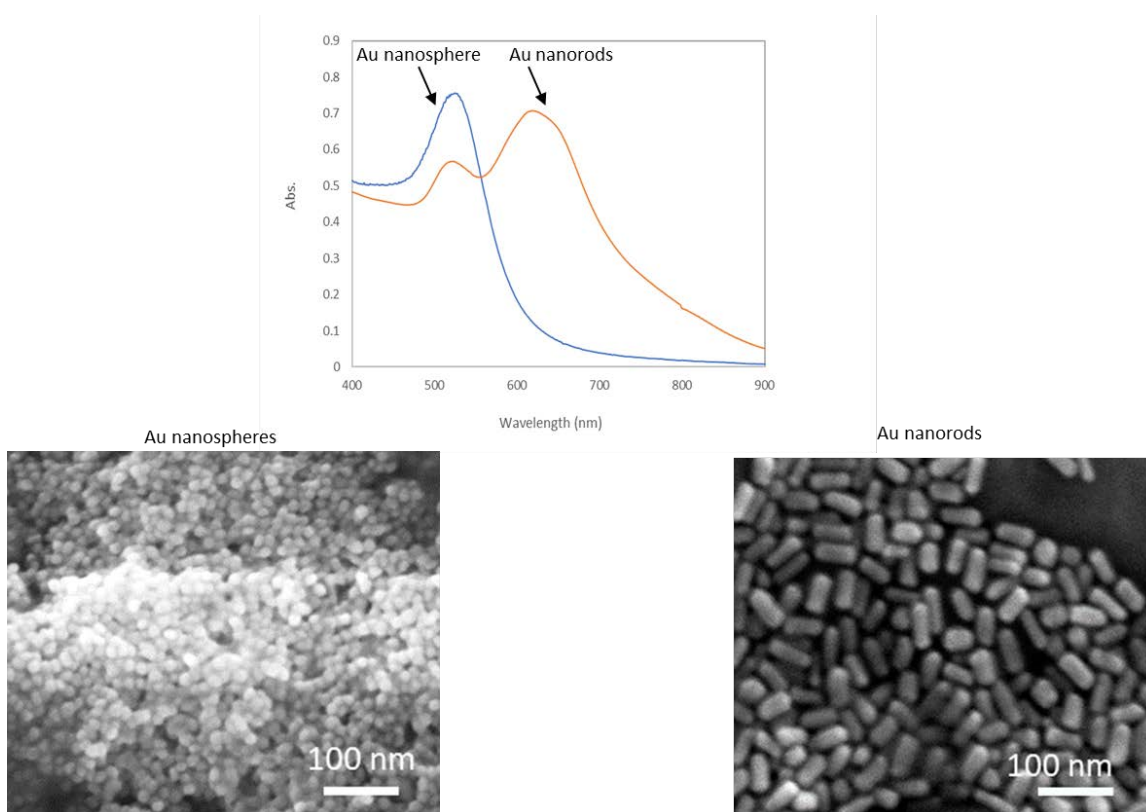


Figure B-1. H<sub>2</sub>O removal rate versus 450 nm LED illumination intensity

### Appendix C. Nanoparticle Testing

As described in the introduction, nanoparticles interact with light more strongly than their bulk counterparts, which can lead to enhanced light absorption and subsequent stronger surface contamination removal through local heating and photo-chemical effects. Additionally, nanoparticles can shift the response wavelength to higher or lower wavelengths, depending on their size and structure, which could lead to effective photo-removal of surface contamination using visible light instead of UV. Thus, nanoparticles were investigated for their potential use in photo-cleaned ion chambers. **Figure C-1** shows representative scanning electron microscopy (SEM) images of gold nanospheres and gold nanorods, along with their UV-visible absorption spectra. The gold nanospheres have a single absorption peak around 520 nm. The gold nanorods have two absorption peaks, one around 520 nm and the other centered around 630 nm, corresponding with the transverse and longitudinal plasmonic modes, respectively. Note, that these spectra were obtained in solution and will shift to lower wavelengths in air.



**Figure C-1. SEM images of gold nanospheres and gold nanorods and their UV-visible absorption spectra.**

Gold nanospheres were drop-cast onto the surface of clean gold coated QCM crystals, and the mass uptake on the surface was measured in  $N_2/H_2O$  flow. The results are presented in **Figure C-2**. As can be seen the gold nanosphere surface uptakes water much more quickly than a smooth bulk gold surface. However, the  $H_2O$  removal rate was found to be  $0.006 \mu\text{g}/\text{cm}^2 \text{ s}$ , which is about  $10\times$  better than bulk gold. Also, the optimal wavelength for photo-desorption was found to shifted toward the nanoparticle resonance wavelength (450 nm versus 365 for bulk gold). Thus, nanoparticles offer the opportunity to adjust and tune the surface properties of materials for enhanced photo-cleaning.

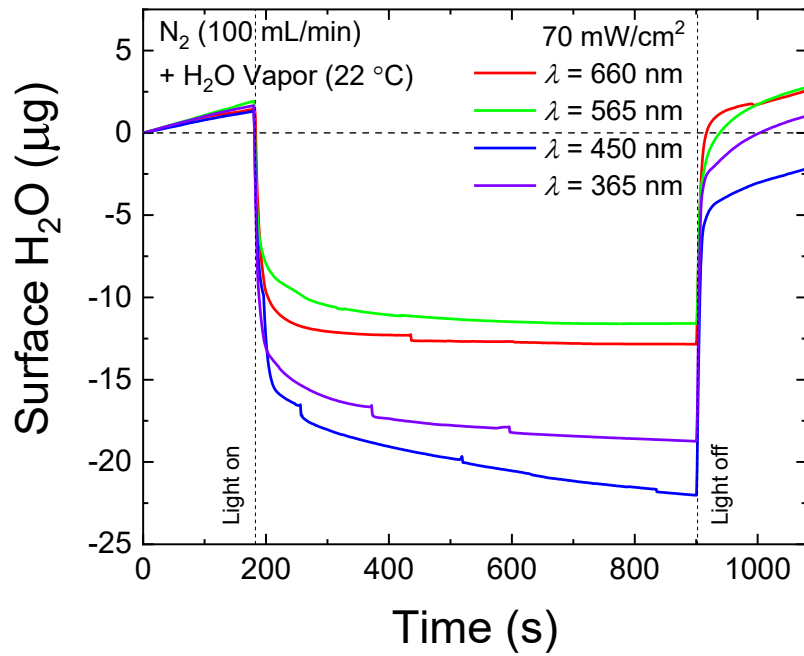


**Figure C-2. Measurements of photo-desorption of water from gold nanosphere coated QCM crystals**

#### Appendix D. References for the Appendices

1. Traub, R. and G. Jensen, *Tritium radioluminescent devices*, *Health and Safety Manual*. 1995, Pacific Northwest Lab., Richland, WA (United States).
2. Nishikawa, M., et al., *Ionization chamber system to eliminate the memory effect of tritium*. Nuclear Instruments and Methods in Physics Research Section A: Accelerators, Spectrometers, Detectors and Associated Equipment, 1989. **278**(2): p. 525-531.
3. Shank, K. and C. Easterly, *Tritium instrumentation for a fusion reactor power plant*. 1976, Oak Ridge National Lab.
4. Seifert, C.E., et al., *Mitigation of memory effects in beta scintillation cells for radioactive gas detection*. Proceedings of the 27th Seismic Research Review: Ground-Based Nuclear Explosion Monitoring Technologies, 2005: p. 804-814.
5. Sheen, S., *NRC Job Code V6060: Extended in-situ and real time monitoring. Task 4: Detection and monitoring of leaks at nuclear power plants external to structures*. 2012, Argonne National Lab.(ANL), Argonne, IL (United States).
6. Röllig, M., et al., *Activity monitoring of a gaseous tritium source by beta induced X-ray spectrometry*. Fusion Engineering and Design, 2013. **88**(6): p. 1263-1266.
7. Knoll, G.F., *Radiation detection and measurement*. 2010: John Wiley & Sons.
8. Worth, L., et al., *Development of a novel contamination resistant ion chamber for process tritium measurement and use in the JET first trace tritium experiment*. Fusion science and technology, 2005. **48**(1): p. 370-373.
9. Vig, J.R., *UV/ozone cleaning of surfaces*. Journal of Vacuum Science & Technology A, 1985. **3**(3): p. 1027-1034.
10. Zion, B.D. and S.J. Sibener, *UV Photodesorption of Novel Molecular Beam Induced NO Layers on NiO(111)/Ni(111)*. The Journal of Physical Chemistry C, 2008. **112**(15): p. 5961-5965.
11. Brongersma, M.L., N.J. Halas, and P. Nordlander, *Plasmon-induced hot carrier science and technology*. Nature nanotechnology, 2015. **10**(1): p. 25-34.

**Distribution:**

*The standard distribution of all  
technical reports is:*

[david.crowley@srnl.doe.gov](mailto:david.crowley@srnl.doe.gov)

[a.fellinger@srnl.doe.gov](mailto:a.fellinger@srnl.doe.gov)

[samuel.fink@srnl.doe.gov](mailto:samuel.fink@srnl.doe.gov)

[connie.herman@srnl.doe.gov](mailto:connie.herman@srnl.doe.gov)

[brady.lee@srnl.doe.gov](mailto:brady.lee@srnl.doe.gov)

[john.mayer@srnl.doe.gov](mailto:john.mayer@srnl.doe.gov)

[cj.bannochie@srnl.doe.gov](mailto:cj.bannochie@srnl.doe.gov)

[Amy.Ramsey@srnl.doe.gov](mailto:Amy.Ramsey@srnl.doe.gov)

[William.Ramsey@SRNL.DOE.gov](mailto:William.Ramsey@SRNL.DOE.gov)

[michael.stone@srnl.doe.gov](mailto:michael.stone@srnl.doe.gov)

[david.babineau@srnl.doe.gov](mailto:david.babineau@srnl.doe.gov)

Records Administration (EDWS)